J Nanopart Res (2018) 20: 209
https://doi.org/10.1007/s11051-018-4307-2

RESEARCH PAPER

A sampler designed for nanoparticles and respirable particles with direct analysis feature

Candace Su-Jung Tsai · Daniel Theisen

Received: 2 April 2018 / Accepted: 23 July 2018 / Published online: 3 August 2018

Abstract A sampler has been designed to collect particles in the nanometer and respirable sizes directly onto a membrane filter and transmission electron microscopy (TEM) grid. The novel design aspects of this sampler include the selection of the diameter of the inlet probe, geometry of the sampler, and the resulting air flow to the sampler. Together, they control the cutoff diameter, which was determined experimentally to be a mass median aerodynamic diameter (MMAD) of 3.8 μm. The maximum aerodynamic diameter entering the sampler is designed to be approximately 8 μm. Nanometer-sized particles are collected on both the filter and grid through diffusion, as confirmed by testing with aluminum oxide engineered nanoparticles collected on the filter which measured a count median diameter (CMD) of 500 nm and a geometric standard deviation (GSD) of 1.97. The primary particles and small agglomerates collected on the grid have a CMD of 100 nm and GSD of 2.3. This diffusion sampler collected close to, if not 100%, of the particles entering the sampler. The sampler is easily wearable for personal exposure and environmental sampling, operates at 0.3 L/min, and can collect particles in various settings at indoor and outdoor environments. Particles are analyzed directly by transmission electron microscope on the grid and by scanning electron microscope on the filter to assess the exposure through particle counts and elemental composition analysis.

Keywords Nanoparticle · Sampler · Diffusion · Respirable · Personal sampling · Microscope analysis · Environmental and health effects

This article is part of the topical collection: 20th Anniversary Issue: From the editors

Nicola Pinna, Executive Editor, Mike Roco, Editor-in-Chief

Electronic supplementary material The online version of this article (https://doi.org/10.1007/s11051-018-4307-2) contains supplementary material, which is available to authorized users.

C. S.-J. Tsai (✉) · D. Theisen
Department of Environmental & Radiological Health Sciences, College of Veterinary Medicine & Biomedical Sciences, Colorado State University, 1681 Campus Delivery, Fort Collins, CO 80523-1681, USA
e-mail: Candace.Tsai@colostate.edu

Introduction

Due to the increasing awareness of potential harm by nanomaterials (Roco 2003; Oberdörster 2004; NSTC 2006; Fleischer and Grunwald 2007; Maynard 2007; Simeonova et al. 2007; Singh and Nalwa 2007; Schulte et al. 2008; Warheit et al. 2008; Roco 2011), the number of studies investigating toxicological effects of nanomaterials has increased greatly in recent years. The risk of potential harm to the environment and humans from selected nanomaterials has been studied and concerns have been raised (Shvedova et al. 2003; Maynard et al. 2004; Methner et al. 2007; Simeonova et al. 2007; NIOSH 2008, 2009; Johnson et al. 2010; Lee et al. 2010; Cena and Peters 2011; Kuhlbusch et al. 2011; Dahm et al. 2012; Lo et al. 2012; Methner et al. 2012; Takagi et al. 2008, 2012; NIOSH 2011, 2013).

Airborne nanomaterials can expose humans through inhalation, and such nanoparticle exposures are typically assessed using some form of a particle sampler.

Size-selective sampling is critical to separate nanoparticles from large particles for collection. The traditional respirable filter sampler relies on a nylon cyclone to pre-separate particles in the respirable size range in order to measure respirable mass exposure. Aerosol particles frequently have a net charge; Briant and Moss (Briant and Moss 1984) found that if the cyclone itself has a net charge, particles with the same charge will be repelled by the electric field created around the cyclone body and be repelled from the cyclone inlet, decreasing their sampling efficiency and underestimating respirable mass. This issue will profoundly affect measurements of nanoparticles.

Several samplers designed to collect nanoparticles have become available since 2010, including the electrostatic precipitation sampler (ESP) (Miller et al. 2010), thermophoretic sampler (TPS) (Leith et al. 2014), personal nanoparticle sampler (PENS) (Tsai et al. 2012), and nanoparticle respiratory deposition (NRD) sampler (Cena et al. 2011), which use various particle deposition mechanisms including electrostatic precipitation, thermophoretic precipitation, diffusion, and impaction. These samplers collect nanoparticles on a filter, mesh screen, or transmission electron microscopy (TEM) grid.

Two broad approaches can be used to collect nanoparticles on grids, i.e., indirect methods and direct methods. Indirect methods have been the usual method used since the 1990s, as in NIOSH Method 7402, Asbestos by TEM (NIOSH 1994). Indirect methods, however, have disadvantages including particle transfer, labor intensity, and the potential for particle agglomerate changes through the preparation process. The shortcomings of the indirect methods have led scientists to experiment with various methods to directly deposit nanoparticles from the air onto a grid, which is the approach used by the ESP and TPS samplers. Grids can be taken from the collection device and placed directly into a transmission electron microscope for analysis. Two significant disadvantages of the ESP and TPS devices are as follows: (1) they are designed to only collect particles with diameters smaller than a micrometer in the nanometer size range, and (2) only some of the particles drawn into each device actually collect on the grid; the rest pass out with the exhaust air.

The sampler described here overcomes both of these shortcomings. This sampling cassette, named Tsai diffusion sampler (TDS), was designed with the novelty of using a specified inlet diameter, cassette housing shape, designed internal height of cassette, and specific airflow to control the cutoff diameter of collected particles so that only respirable particles are sampled. The diffusion mechanism, used for this TDS, is also used by the Naneum wide range aerosol sampler (WRAS) (Gorbunov et al. 2009) and the NRD sampler (Cena et al. 2011); however in these devices, the nanoparticles are deposited onto wire meshes or a nylon mesh screen rather than TEM grids. With the TDS, the grid collects mostly primary and small agglomerates of submicrometer nanoparticles via Brownian motion when air flows across the top of the filmed grid. The polycarbonate filter collects particles over a wide size range via diffusion and sieving as air flows through the filter pores, such that many nanoparticles and all of the larger particles are collected on the filter surface between pores.

Design and methods

This TDS is designed to collect particles in the nanometer and respirable size ranges with the aerodynamic cutoff diameter of approximately 3.8 μm, determined experimentally, for respirable particles. The design has been filed for patent. The particle size entering the sampler cassette is determined by a combination of the inlet nozzle size and the sampling air flow. As demonstrated by others (Su and Vincent 2004), the aspiration efficiency of a plain round inlet such as the inlet nozzle at the top of the cassette as shown in Fig. 1a follows a sigmoidal curve similar to the respirable pre-separator curve. The cutoff diameter of the curve is a function of the inlet diameter and air flow, and must be determined experimentally. The sampler inlet was designed so that the inlet aspiration efficiency is minimally affected by sampling direction (upward, horizontal, or downward); this was also reported in the study by Su and Vincent (Su and Vincent 2004). Using the inlet nozzle of a sampling cassette as a pre-separator is also the design principle of the Institute of Medicine (IOM) inhalable mass sampler. By experimentally determining the proper combination of inlet diameter and air flow, the IOM filter cassette aspiration efficiency closely matches the American Conference of Governmental Industrial Hygienists (ACGIH) inhalable mass sampling criterion.

The design approach of the TDS (Fig. 1a) is capable of meeting the performance requirement of a personal sampler that can measure both the nanometer and micrometer portions of the respirable particles from microscope images; and provide direct sampling and analysis on collected particles using microscopy.

The novel geometry design of the TDS includes (1) 2-mm-diameter circular-bell shape air inlet with a nozzle length of 10 mm, (2) 6-mm distance between grid substrate to the inlet opening at the top part of a 25-mm-diameter cassette housing (which meets the recommended design criterion of Hinds (Hinds 1999)), and (3) smooth curved shape of top cassette housing, to provide smooth air streamline for particle moving from inlet toward the sampling substrate- filter and grid. The dimension of geometry design is shown in Fig. 1b. Together with the design air flow, these factors determine the sizes of particles entering the sampler and thus the cutoff diameter of particles collected on the two substrates. The TDS substrates consist of a 25-mm diameter, 0.22-μm pore size polycarbonate membrane filter (Isopure, Millipore Sigma, Burlington, MA, USA) (Sigma n.d.) with a TEM-copper grid in 400 mesh with SiO_2-coated film (SPI, West Chester, PA,USA) attached to the center of the filter (Fig. 1a, c). The polycarbonate membrane filter gives the ease to analyze collected particles on the filter using scanning electron microcopy (SEM). It is operated using a personal sampling pump (Gil-Air 3 personal sampling pump, St. Petersburg FL, USA) running at 0.3 L/min air flow (Fig. 1c), pulling particles in the air through the 2-mm-diameter circular inlet into the cassette housing. Particles are then collected on both the grid and filter (Fig. 1a, c).

The sampler was designed using Autodesk Inventor 2018 and 3D printed (ProX 500, 3D Systems, Rock Hill, SC, USA) through selective laser sintering (SLS) of nylon powder (DuraForm ProX PA, nylon 12- CAS: 25038-74-8). SLS is extremely prevalent in rapid manufacturing practices where it has proven its utility in the automotive and aerospace industries (Zarringhalam et al. 2006). The ProX 500 system used here is able to efficiently manufacture ready to use functioning parts with high resolution and dimensional accuracy (Systems 2017).

Particle deposition on grid

As shown in Fig. 1a, a TEM-copper filmed grid was taped onto a 25-mm-diameter filter. A metal support screen was used to support the polycarbonate filter. Air was drawn through the filter and aerosol particles deposited on the grid via Brownian diffusion. Theoretically, a particle's diffusion is a function of its diffusion coefficient, D, given by the Stokes-Einstein equation:

$$D = \frac{kTC_c}{3\pi\eta d_p} \tag{1}$$

In this equation, k is Boltzman's constant, T is the absolute temperature, C_c is the Cunningham slip correction factor, η is the gas viscosity, and d_p is the particle diameter.

At standard conditions (constant temperature and viscosity), a particle's diffusion coefficient depends only on its diameter and, as expected, the diffusion increases as the diameter decreases. Since Brownian motion is random, a collection of aerosol particles of the same diameter will be displaced different distances along an arbitrary axis in any given time interval. The distance particles travel under Brownian motion approximates a normal distribution; the root mean square (rms) average distance for a collection of particles' movement in time t by definition is equal to the standard deviation (σ) of the distribution and is given by Eq. 2 (Hinds 1999).

$$\sigma = X_{\mathrm{rms}} = \sqrt{2Dt} \tag{2}$$

Thus, according to Eqs. 1 and 2, during the time t that a particle spends passing the grid, smaller particles can expect to travel a larger average distance than larger ones, so that greater numbers (portion) of smaller particles would be expected to be found on the grid. Thus, nanoparticles, due to their large Brownian displacement, have a high probability of striking a TEM grid element as they pass by the grid; this is illustrated by the following calculations.

At the typical pump air flow of 0.3 L/min through this TDS 25-mm-diameter filter cassette (23 mm diameter of filter collecting area), the air flows toward the grid at a velocity of approximately 1 cm/s. Air streamlines striking the center of the grid will be directed toward the edges of the grid; since the grid has a radius of 1.5 mm, air striking the center of the grid will take approximately 0.15 s to reach the edge. Solving Eqs. 1 and 2, a 10-nm-diameter particle, for example, has an rms displacement (X_{rms}) of 0.13 mm in 0.15 s. Since the X_{rms} is also by definition its standard deviation, and 32% of any distribution values are greater than the standard deviation, 32% of the particles will have moved farther

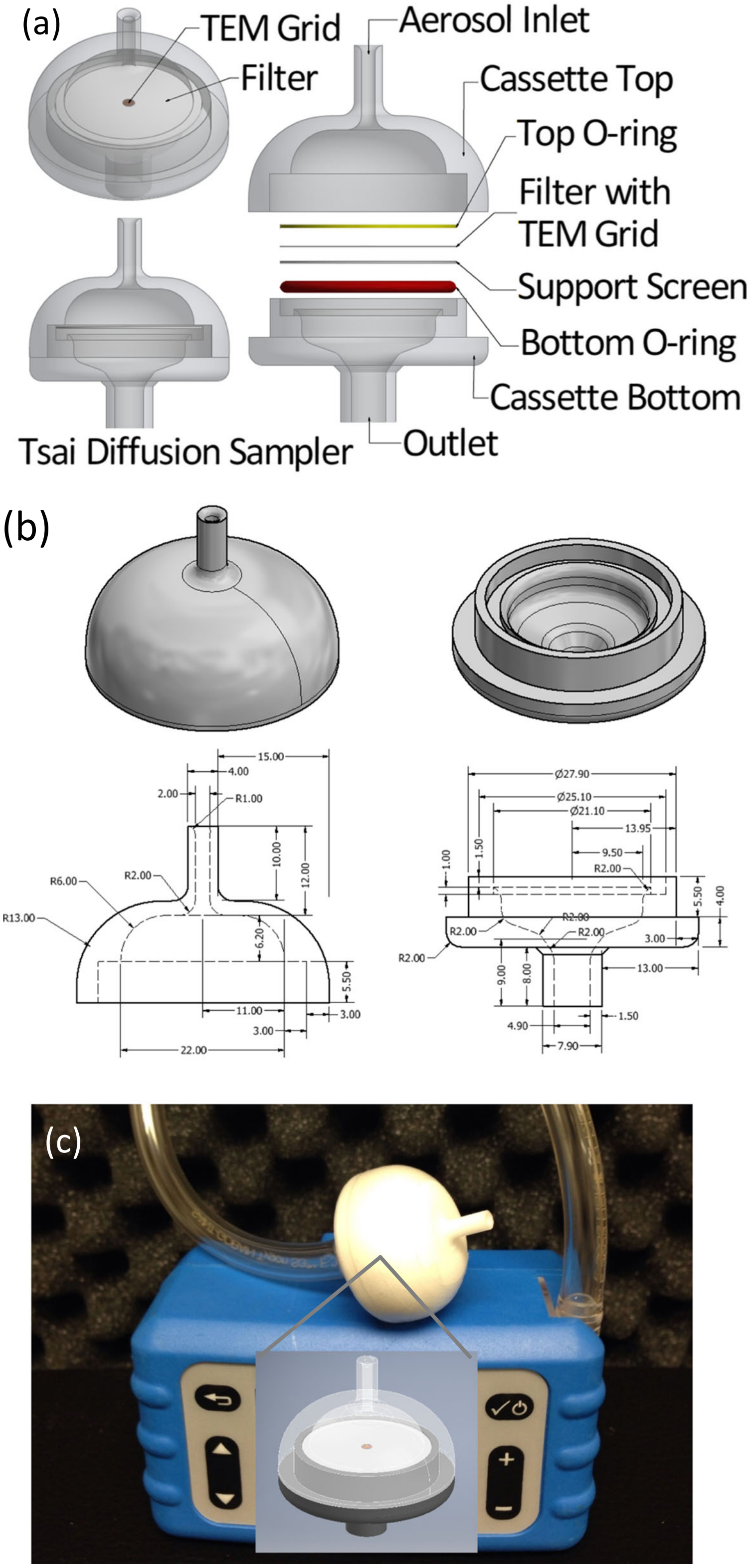

Fig. 1 Tsai diffusion sampler (TDS). **a** Illustration of sampler design and components. **b** Geometry of top and bottom cassette. **c** 3D-printed nylon TDS connects to a sampling pump with the grid and filter substrate inside TDS. Note: dimension of cassette is shown in mm. *R* is radius and ϕ is diameter

than this distance while passing over the grid. Half of these particles will move away from the surface of the grid and half of them (16%) will move toward the surface of the grid and deposit on the filmed opening space of the grid. Thus, 10-nm particles traveling on streamlines that pass within a few tenths of a millimeter of the grid surface will have a high probability of being collected. In addition, flow so close to the surface is likely to be in the frictional boundary layer, meaning that the velocities are lower than the free-stream velocities, the residence times are longer, and more collection by diffusion will occur. The calculated rms displacements range from 0.32 mm for a 4-nm-diameter particle to 0.01 mm for a 300-nm-diameter particle as shown in Table 1; thus, particles across the entire nanometer size range will have a measurable displacement while passing over the surface of the grid and particles throughout this size range will deposit on the grid due to diffusion.

These calculations indicate that a significant number of the nanometer-sized particles in the air flow impinging on the grid will move to the grid surface and be collected. This particle deposition process has been confirmed experimentally in numerous laboratory and field measurements, described below.

Table 1 Particle diameters and corresponded parameters including diffusion coefficient (D), coefficient of diffusion collection (N_D), efficiency of diffusion (E_D), and root mean square displacement (X_{rms})

d (μm)	D (m²/s)	N_D	E_D	X_{rms} (mm)
0.004	3.35E-07	9377.3	1.00	0.32
0.005	2.15E-07	6018.3	1.00	0.25
0.006	1.5E-07	4198.8	1.00	0.21
0.008	8.46E-08	2368.1	1.00	0.16
0.01	5.45E-08	1525.6	1.00	0.13
0.015	2.45E-08	685.8	1.00	0.09
0.02	1.4E-08	391.9	1.00	0.06
0.03	6.39E-09	178.9	1.00	0.04
0.04	3.69E-09	103.3	1.00	0.03
0.05	2.43E-09	68.0	1.00	0.03
0.06	1.73E-09	48.4	1.00	0.02
0.08	1.03E-09	28.8	1.00	0.02
0.1	6.94E-10	19.4	1.00	0.01
0.15	3.51E-10	9.8	1.00	0.01
0.2	2.23E-10	6.2	1.00	0.01
0.3	1.23E-10	3.4	1.00	0.01
0.4	8.31E-11	2.3	1.00	0.00
0.5	6.24E-11	1.7	1.00	0.00
0.6	4.98E-11	1.4	0.99	0.00
0.8	3.54E-11	1.0	0.98	0.00
1	2.74E-11	0.8	0.95	0.00

Particle deposition on polycarbonate filter

Particles that enter the sampler housing through the inlet probe are distributed onto the filter, and particle agglomerates larger than the pore size (~220 nm) are deposited by sieving. Particles smaller than the pore size will be deposited onto the filter surface between pores by Brownian motion.

The Nuclepore polycarbonate filter, also known as a membrane filter, has been available since the 1940s, and its properties have been verified (Spurny et al. 1969). The efficiency of diffusion on the membrane filter, E_D, can be calculated by Eq. 3 (Twomey 1962; Spurny et al. 1969) below when the coefficient of diffusive collection, N_D, shown in Eq. 4 (Spurny et al. 1969), is greater than 0.01.

$$E_D = 1-0.081904\, e^{-3.6568\, N_D}-0.09752\, e^{-22.3045\, N_D} -0.03248\, e^{-56.95\, N_D}-0.0157\, e^{-107.6\, N_D}-\ldots \quad (3)$$

The remaining terms in Eq. 3 will approach zero. The coefficient of diffusive collection is given by:

$$N_D = \frac{\mathrm{LDP}}{R_0^2\, q} \quad (4)$$

where L is the filter thickness (m), D is the diffusion coefficient (Eq. 1), P is the filter porosity, R_0 is the pore radius of clean filter (m), and q is the face velocity of air at filter (m/s).

For this sampler design, the 0.22-μm porous polycarbonate filter has a thickness of 25 μm (Sigma), porosity of 13.8%, pore radius of 0.11 μm, and q of 0.01 m/s. The diffusion efficiency of the filter is 100% for particles with diameters of 500 nm (0.5 μm) or smaller, and greater than 95% for particles of 1 to 0.5 μm as shown in Table 1. Particles with diameters greater than the pore size (220 nm) will of course be collected with 100% efficiency.

The particle's motion entering the sampler inlet and inside the housing can be characterized using the Stokes number (Stk), Eq. 5 (Hinds 1999). In this equation, τ is the relaxation time (s), calculated using Eq. 6, U_0 is the air velocity, and d_c is the cylinder diameter of airflow which has been analyzed separately for both the inlet probe diameter (2 mm) and the cassette housing (23 mm) diameter.

$$\text{Stokes number } (Stk) = \tau \frac{U_0}{d_c} \tag{5}$$

$$\tau = \frac{\rho_p \, d_p^2 \, C_C}{18 \, \eta} \tag{6}$$

where ρ_p is particle density (kg/m^3).

When Stk >> 1, particles continue moving in a straight line when the air turns; when Stk << 1, particles follow the air streamlines perfectly (Hinds 1999). The particle motion behavior at the probe inlet determines the particle sizes entering the inlet as they follow and deviate from the air streamlines. This determines the maximum size of particles to be sampled by this device, i.e., the largest particle that can follow the sharply curving streamlines at the device inlet.

Based on the particle count size distribution, particle characteristics can be analyzed using the following equations. Geometric mean diameter, d_g, is calculated using Eq. 7 (Hinds 1999). Geometric standard deviation, σ_g, is calculated using Eq. 8 (Hinds 1999).

$$\ln d_g = \frac{\sum n_i \ln d_i}{N} \tag{7}$$

$$\ln \sigma_g = \left(\frac{\sum n_i \left(\ln d_i - \ln d_g \right)^2}{N-1} \right)^{1/2} \tag{8}$$

Count median diameter (CMD) is obtained from cumulative percentile graph of particles at 50% cumulative particle size. CMD is converted to mass median diameter (MMD) of specific particle such as for aluminum oxide particles utilizing the Hatch-Choate conversion equation (Eq. 9) (Hinds 1999). The mass median aerodynamic diameter (MMAD) is calculated using Eq. 10 (Hinds 1999).

$$\text{MMD} = \text{CMD} \; e^{3 \, ln^2 \sigma_g} \tag{9}$$

$$d_a = d_p \left(\frac{\rho_p}{\rho_0} \right)^{\frac{1}{2}} \tag{10}$$

Where d_a is aerodynamic diameter, d_p is particle diameter, ρ_p is particle density, and ρ_0 is standard particle density which is 1 g/cm^3.

Particle collection and analysis protocol

Crystalline aluminum oxide (Al_2O_3) nanopowder (Nanodur, Nanophase, Romeoville IL, USA), with a density of 3600 kg/m^3 and primary particle size of 40 nm, was used as a test aerosol to determine the particle size distribution of collected particles in the TDS. This nanopowder was chosen because of the wide range of aerosol particle sizes from individual primary particles to small and large agglomerates, and the ease of aerosolizing the particles. The expansion of sampling other nanoparticles using TDS is promising since the collection is driven by the airflow drag force and the inertia momentum of particle to control the moving direction of particle, and collected particle cutoff size is based on the aerodynamic diameter.

The experimental setup is illustrated in Fig. 2. Powder was aerosolized inside an ultra-filtered glove box (Terra Universal, Fullerton CA USA, 89 cm × 61 cm × 64 cm) through agitation by stirring 200 mL of aluminum oxide in a container with a compact digital mixer operating at 2000 rotations per minute (rpm) (Cole-Parmer, Vernon Hills IL, USA). The agitator, powder, and sampling cassettes were placed inside the glovebox at center area (Fig. 2), and the aluminum oxide aerosols were diffused to the top opening of the container and pulled into samplers and instruments. Two direct reading real-time instruments (RTIs) were utilized to measure particle number concentrations and size distributions over a range of 10 nm to 10 μm. An optical particle sizer (OPS) (Model 3330, TSI, Shoreview, MN, USA), which measures particles from 0.3 to 10 μm, and a scanning mobility particle sizer (SMPS) (Model 3910, TSI, Shoreview, MN, USA), which has a measuring range of 10 to 420 nm, collected side by side with 1-min measurement intervals. The RTIs were sampled through 1 m of conductive tubing. The RTIs and three identical TDS samplers were positioned equidistant from each other and 5 cm away in both height and distance from the source (Fig. 2). The air velocity at the sampling area ranged from 1 to 7.6 cm/s (2 to 15 ft/min) for horizontal direction and from 0 to 3 cm/s (0 to 6 ft/min) for vertical direction. The glove box and all experimental equipment were decontaminated with clean room wipes and distilled water prior to experimentation.

The RTIs initiated sampling 10 min prior to aerosol generation to establish background concentrations. Directly following this, the three personal sampling pumps

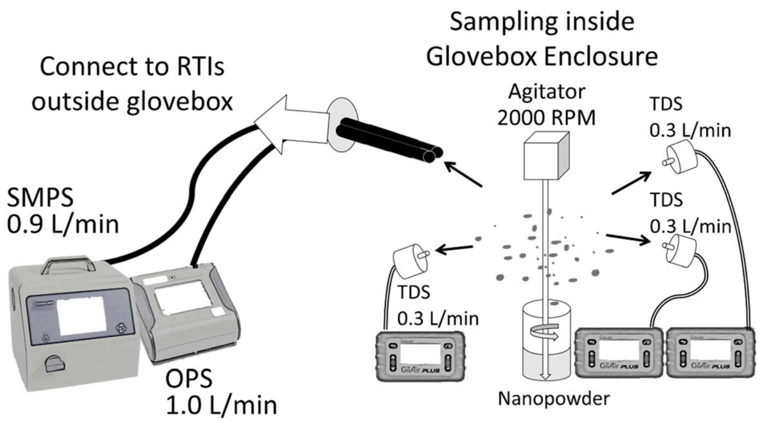

Fig. 2 Illustration of experimental set up for laboratory particle sampling. Note: The RTIs and three identical TDS samplers were positioned equidistant from each other and 5 cm away in both height and distance from the source

and the compact digital mixer were activated. Aerosol generation was conducted for 40 min. Following the sampling period, 10 min of post experimental background was measured with the RTIs. The RTI data was exported to an Excel spreadsheet where it was analyzed.

The TDS TEM grid and filter samples were analyzed with TEM (JOEL JEM-2100F) and SEM (JOEL JSL-6500F), respectively. The following TEM imaging protocol was utilized to analyze grid: (1) five low magnification (× 50) images were taken to encompass the entire grid (center, and four quadrants); (2) four grid spaces were selected equidistant two spaces from the grid center, these spaces were imaged at × 500; (3) the chosen grid spaces were imaged by traversing (9–12 images per grid) the grid space at × 5000 until 300 particles were imaged. For filter analysis using SEM, the filters were prepared by cutting a 1/8th slice of the filter and coating with 10 nm of gold. Three sections of the filters were imaged (center, middle, and edge) at × 9000–25000 until 300 particles were imaged per sample. Particle images were analyzed using FIJI (Schindelin et al. 2012) imaging software to count and measure particle size. The particle sizes were organized following 13 bin ranges within 10 to 420 nm and 14 bin ranges above 420 nm to 10 μm, similar to two RTIs bin ranges, to plot particle count frequency with size distribution and cumulative percent particle counts.

Results and discussion

The aluminum oxide particles with an average primary size of 40 nm diameter were found to be easily aerosolized and dispersed; they appeared with small primary particles less than 40 nm and agglomerates ranged in nanometer to micrometer sizes. The sampling tests demonstrated a practical exposure scenario where the aerosol concentration varied, with some higher concentrations in some time intervals. The aluminum oxide total particle number concentrations measured throughout the sampling time period is presented in Fig. 3a. The average size distributions of aluminum oxide particles were presented in Fig. 3b. The standard deviation data of concentrations at each size bin were presented in Table S1 (Supplementary Information). Instrument measurements were used to evaluate the particle concentration levels and referenced particle sizes for tests. The size distributions of generated airborne aluminum oxide particles measured by SMPS were shown in the size range from 10 to 420 nm with the mode size measured to be 154 nm. The OPS measurements showed increasing concentrations at sizes close to 0.3 and 10 μm but showed low concentrations around 1 μm (Fig. 3b). The average particle number concentration during 62 min (62 data) of sampling measured by SMPS (10–420 nm) and by OPS (0.3–10 μm) were 237 particles/cm^3 and 7 particles/cm^3, respectively. The peak emission showed concentrations in a range from about 50 to greater than 4000 particles/cm^3 for particles smaller than 420 nm; and the particle counts for larger particles above 0.3 μm ranged from a few particles to about 80 particles/cm^3. The particle counts were aluminum oxide particles only with essentially 0 particles from the ambient background in the filtered glove box. These concentrations are representative exposure levels in the environmental setting.

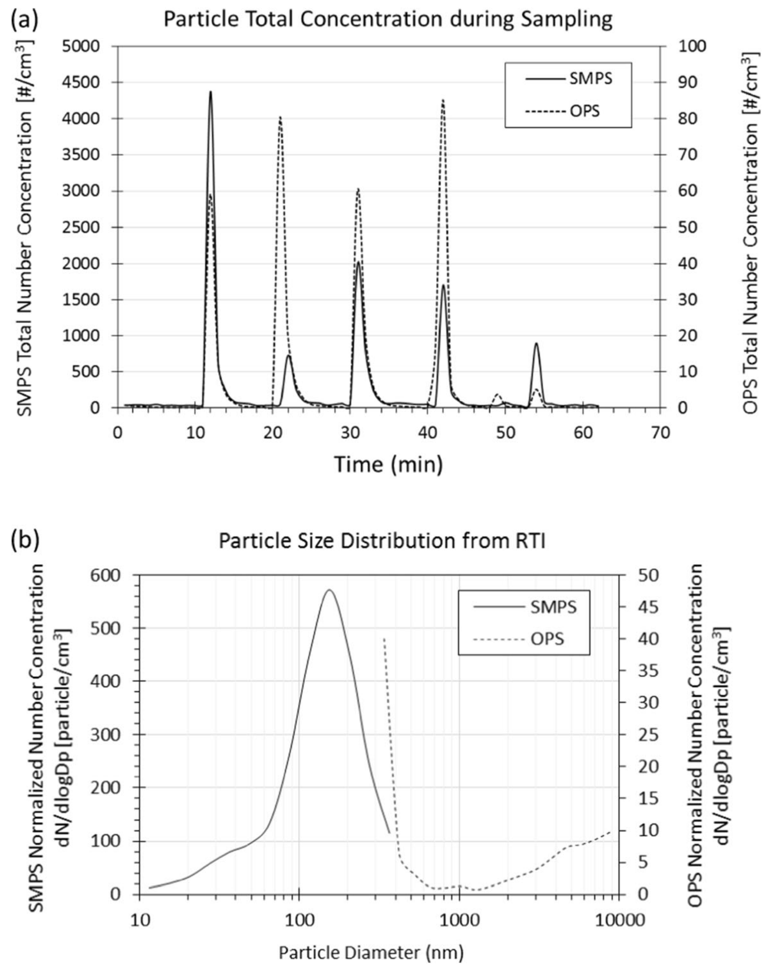

Fig. 3 Aluminum oxide particles measured using SMPS and OPS during experiment period. **a** Total particle number concentration. **b** Particle size distributions with mode size at 154 nm measured by SMPS. Note: Average particle total number concentration during 62 min of sampling measured by SMPS (10–420 nm) and by OPS (0.3–10 μm) are 237 and 7 particles/cm^3 respectively

Collected particles on the filter and grid were analyzed separately using SEM and TEM. Typical particle images are presented in Fig. 4. Small particles and agglomerates similar to or smaller than the pore size of filter were collected between pores and/or trapped on pores (Fig. 4a, b). Agglomerates were observed as well (Fig. 4a). The TEM grid collected particles on the grid space. Many particles were seen in Fig. 4c in which most were primary particles or small agglomerates (Fig. 4d).

Numerous images of particles on filter and grid spaces were taken to obtain a minimum of 300 particles being counted and analyzed to obtain their sizes. The averages of three sets of sample analyses were calculated. The results are plotted in a cumulative percentile graph versus particle diameters in Fig. 5a. Particles on the filter range in size from 36 to 5800 nm, and particles on grid spaces range in size from 15 to 1560 nm. The particle mean diameters are 793 and 130 nm for aluminum oxide particles on the filter and grid spaces, respectively. The particle count size distribution and characteristics were summarized in Table 2. Data were calculated using Eqs. 7 to 10.

For aluminum oxide particles collected on the polycarbonate filter of this sampler, the CMD was 500 nm (0.5 μm) with GSD of 1.97 and the MMD calculated using Eq. 9 was approximately 2 μm (Table 2). For a lognormal count distribution, d_g is equal to the CMD (Hinds 1999). In Table 2, d_g and CMD differ because the underlying distribution is not actually log-normal as shown in Fig. 5b. The equivalent MMAD of aluminum oxide particles would be approximately 3.8 μm, which is very close to the cutoff diameter of respirable particles (4 μm). The size analysis shown in Fig. 5b when compared to the RTI data in Fig. 3b had smaller particle modes

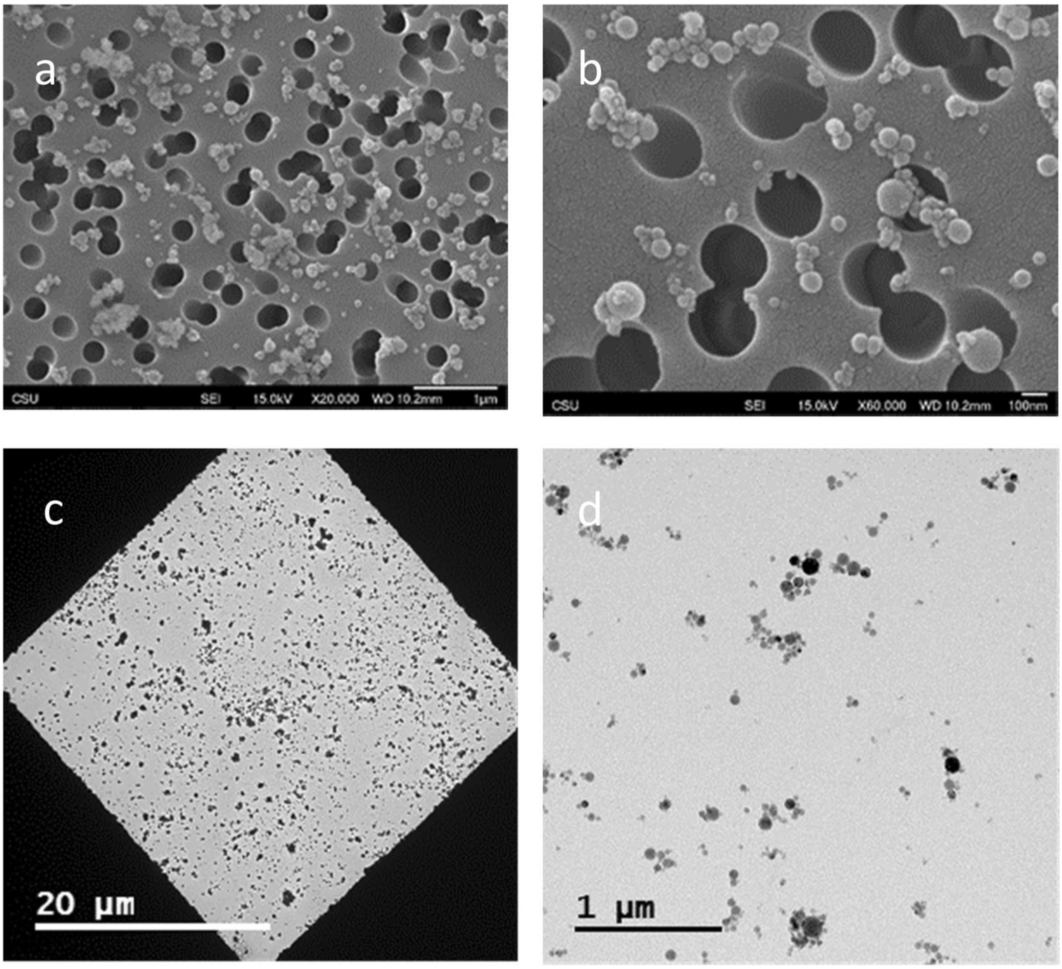

Fig. 4 Images of aluminum oxide particles collected on filter and grid. **a** SEM images of particles collected on filter, × 20,000. **b** SEM images of particles collected on filter, × 60,000. **c** TEM images of particles collected on grid space, × 500. **d** TEM images of particles collected on grid space, × 5000

at 65 and 116 nm (Fig. 5b) compared to the 154 nm measured by the SMPS. The size range of particles from image analysis extended to above 420 nm, the maximum size measured by SMPS. These two measurements cannot be used to directly compare the absolute sizes of measured particles. The reason is that SMPS measured the electrical mobility size of particles, which is correlated with the electrical charge on the surface of three-dimensional particles, to determine particle diameter; however, the size analysis of collected particles is based on two-dimensional particle images used to measure the area of imaged individual particles and agglomerates, which is then used to calculate the diameter of equivalent spherical particles. The OPS shows increased particle concentration toward to the maximum size of 10 μm in Fig. 3b, but the TDS is designed to collect particle sizes up to 8 μm aerodynamic diameter so that larger particle agglomerates do not enter the TDS inlet. Thus, differences between these two measurements are expected. Although variations occurred between different measurement approaches, both SMPS and OPS measurements showed that the range of particles collected on filter and grids were also found being detected by both instruments. TDS provides a wider particle size range for analysis that can overcome the use of multiple instruments (SMPS and OPS). However, it is still recommended to use instrument and TDS together to confirm the particle size being evaluated.

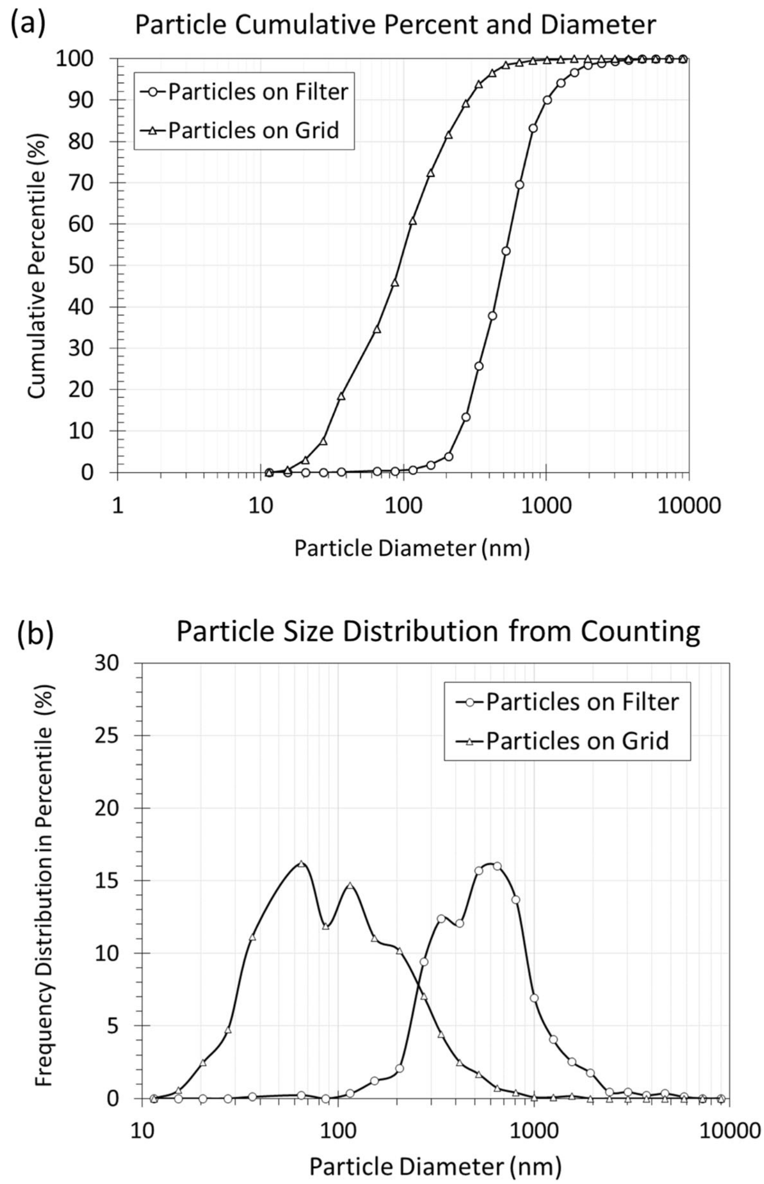

Fig. 5 **a** Aluminum oxide particle cumulative size distribution. **b** Aluminum oxide particle count frequency distribution

Table 2 Characteristics of aluminum oxide particles collected on filter and grid

Al_2O_3 particles	Particles on filter	Particles on grid
Particle mean diameter	793 nm	130 nm
Mean diameter standard deviation	591 nm	127 nm
Geometric mean diameter, d_g	641 nm	92 nm
Geometric standard deviation, σ_g	1.97	2.30
Count median diameter, CMD	500 nm	100 nm
Mass median diameter, MMD	1987 nm	793 nm
Mass median aerodynamic diameter, MMAD	3770 nm	1505 nm

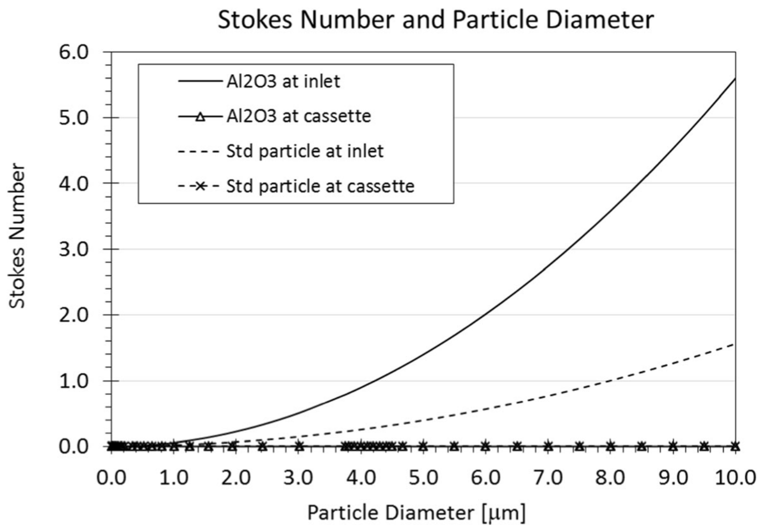

Fig. 6 Stokes number and corresponded particle diameter for aluminum oxide and standard particles at inlet probe and cassette housing

A particle's motion while entering the sampler through the inlet probe and inside the sampler housing will vary by its diameter. This relationship can be interpreted using the particle Stokes number as presented in Fig. 6, based on Eq. 5 and data shown in Table S2 (Supplementary Information). When particles enter the inlet probe, aluminum oxide particles approximately 4 μm or smaller will follow the air streamline since the Stokes number is less than 1. For standard-density particles, diameters approximately 8 μm or smaller will follow the air streamline in the inlet probe, since their Stokes number is less than 1. This determines the maximum particle size entering the sampler probe inlet. Once particles enter into the cassette housing, all Stokes numbers are extremely small for particles 10 μm or smaller; thus, all will follow air streamlines.

Contrary to other nanoparticle samplers, quantitative analysis can be performed using the TDS since approximately 100% of the particles entering the sampler are collected on the filter and grid. The particle number concentration can be estimated from the number of particles counted per image, the area of the grid opening that was imaged, the sampling air flow, and the sampling time period to provide a quantitative analysis of size-fractioned particle concentration. This counting protocol is in current development.

We have further tested this sampler by collecting particles for qualitative analysis in various settings to identify collected particles' morphology and composition using TEM and energy-dispersive X-ray spectroscopy (EDX). They include particles emitted from laser printer printing, handling fumed silica powder, disturbing bulk samples of carbon nanotubes, and particles released from mining activity in an experimental metal mine. Images of such particles collected using the TDS are shown in Fig. 7. The results seen in Fig. 4 demonstrate that the TDS can effectively sample fibrous and non-fibrous particles. Thus, spherical primary particles such as metal, nonmetal or metal-oxide nanoparticles, primary fibrous particles, and agglomerates of all these particles are expected to be collected by the TDS. The theoretical estimation of cutoff diameter for fibrous particles is difficult to estimate due to their high-aspect ratio; the sampler will be further studied experimentally while collecting high-aspect ratio nanoparticles to establish the cutoff particle size and sampling limitations for fibrous particles. The qualitative analysis has also been used by other nanoparticle samplers (Tsai et al. 2009a, b; Miller et al. 2010; Cena et al. 2011; Tsai et al. 2012; Leith et al. 2014; Park et al. 2009).

In addition, electrostatic effects of the nonconductive nylon cyclone used for respirable mass sampling has been of concern for its potential to affect particle collection (Almich and Carson 1974). However, the nylon material used in 3D printing the TDS has successfully collected various aerosols, as described above. The sampler material can be altered if required for collecting conductivity-sensitive substances.

It is a challenge to collect and evaluate trace amount of nanoparticle in the air; TDS collects

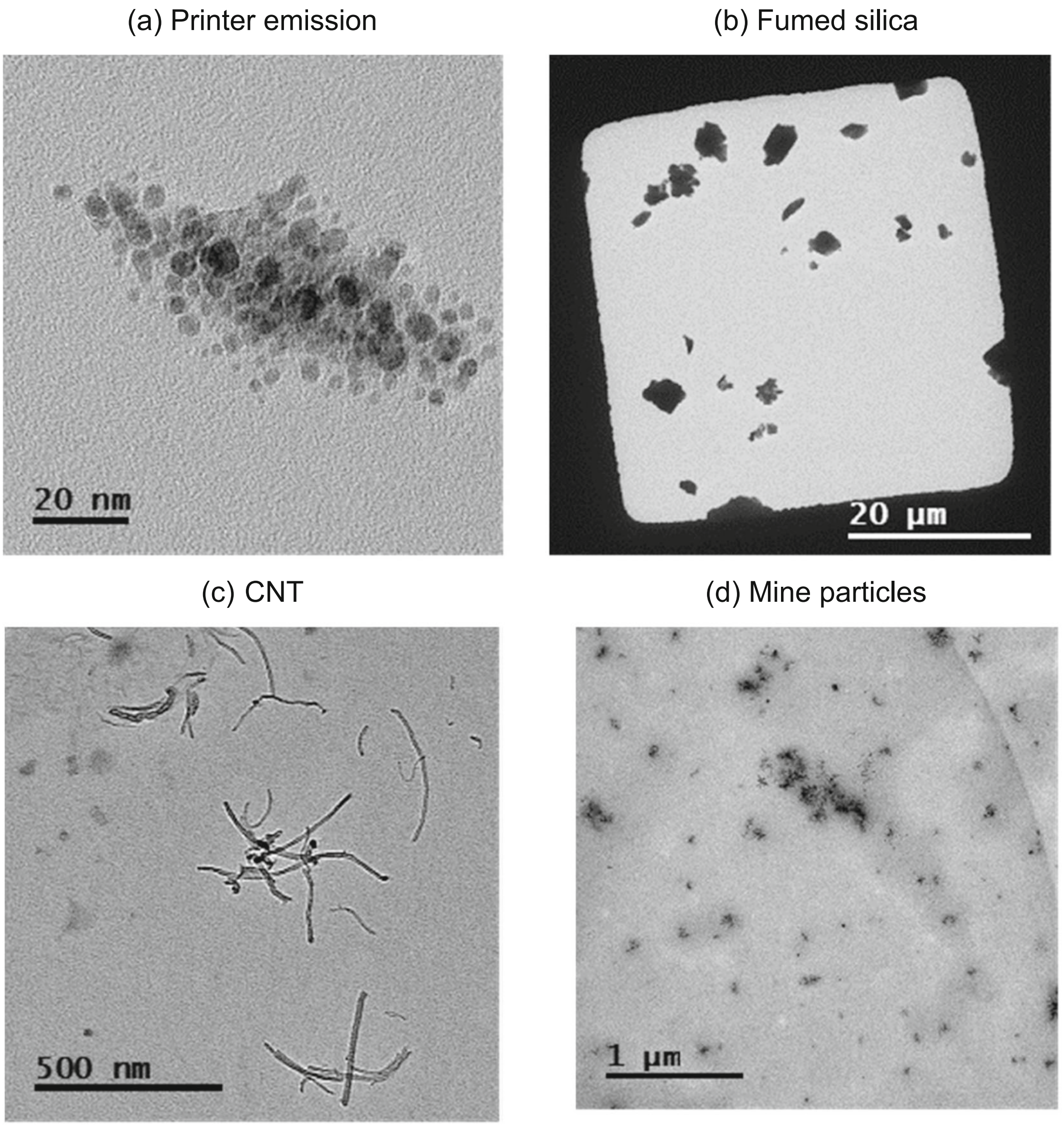

Fig. 7 TEM images of sampling particles using the TDS. **a** Printer emission particles. **b** Fumed silica particles. **c** Carbon nanotube (CNT). **d** Particles from mining activity

nanoparticles at concentrations as low as a few hundred particles per cubic centimeter thus giving the valuable finding about nanoparticle identification. The unique features of the TDS allow for a quantitative analysis of particle number concentration and size distribution that is representative of the particle concentration in the sampled air. This sampler is easily used as a typical personal sampling cassette in the field for personal exposure or environmental sampling.

Acknowledgements The authors acknowledge the financial support of startup fund to Dr. Tsai and patent application by the Colorado State University, and financial support to Daniel Theisen's effort by the Centers for Disease Control and Prevention through grant number 5T42OH009229-11. Authors also thank TSI Incorporated for their collaboration and consultation on instrument operation and maintenance.

Compliance with ethical standards

Conflict of interest The authors declare that they have no conflict of interest.

References

Almich BP, Carson GA (1974) Some effects of charging on 10-mm nylon cyclone performance. Am Ind Hyg Assoc J 35:603–612

Briant JK, Moss OR (1984) The influence of electrostatic charge on the performance of 10-mm nylon cyclones. Am Ind Hyg Assoc J 45(440):440–445

Cena L, Peters T (2011) Characterization and control of airborne particles emitted during production of epoxy/carbon nanotube nanocomposites. J Occup Environ Hyg 8:86–92

Cena LG, Anthony TR, Peters TM (2011) A personal nanoparticle respiratory deposition (NRD) sampler. Environ Sci Technol 45(15):6483–6490

Dahm MM, Evans DE, Schubauer-Berigan MK, Birch ME, Fernback JE (2012) Occupational exposure assessment in carbon nanotube and nanofiber primary and secondary manufacturers. Ann Occup Hyg 56(5):542–556

Fleischer T, Grunwald A (2007) Making nanotechnology developments sustainable. A role for technology assessment? J Clean Prod 16:889–898

Gorbunov B, Priest ND, Muir RB, Jackson PR, Gnewuch H (2009) A novel size-selective airborne particle size fractionating instrument for health risk evaluation. Ann Occup Hyg 53(3):225–237

Hinds WC (1999) Aerosol technology—properties, behavior, and measurement of airborne particles. Wiley-Interscience, New York

Johnson DR, Methner MM, Kennedy AJ, Steevens JA (2010) Potential for occupational exposure to engineered carbon-based nanomaterials in environmental laboratory studies. Environ Health Perspect 118(1):49–54

Kuhlbusch TAJ, Asbach C, Fissan H, Gohler D, Stintz M (2011) Nanoparticle exposure at nanotechnology workplaces: a review. Part Fibre Toxicol 8:1–18

Lee JH, Lee SB, Bae GN, Jeon KS, Yoon JU, Ji JH, Sung JH, Lee BG, Yang JS, Kim HY, Kang CS, Yu IJ (2010) Exposure assessment of carbon nanotube manufacturing workplaces. Inhal Toxicol 22:369–381

Leith D, Miller-Lionberg D, Casuccio G, Lersch T, Lentz H, Marchese A, Volckens J (2014) Development of a transfer function for a personal, Thermophoretic nanoparticle sampler. Aerosol Sci Technol 48(1):81–89

Lo LM, Dunn K, Hammond D, Marlow D, Topmiller J, Tsai S, Ellenbecker M, Huang C (2012) Evaluation of engineering controls in a manufacturing facility producing carbon nanotube-based products. National Institute for Occupational Safety and Health (NIOSH) Division of Applied Research and Technology Engineering and Physical Hazard Branch EPHB Report No. 356-13a

Maynard AD (2007) Weighing Nanotechnology's risks. Flying Blind, New York

Maynard A, Baron P, Foley M, Shvedova A, Kisin E, Castranova V (2004) Exposure to carbon nanotube material: aerosol release during the handling of unrefined single walled carbon nanotube material. J Toxic Environ Health A 67(1):87–107

Methner MM, Birch ME, Evans DE, Ku BK, Crouch K, Hoover MD (2007) Case study: identification and characterization of potential sources of worker exposure to carbon nanofibers during polymer composite laboratory operations. J Occup Environ Hyg 4(12):D125–D130

Methner M, Crawford C, Geraci C (2012) Evaluation of the potential airborne release of carbon nanofibers during the preparation, grinding, and cutting of epoxy-based nanocomposite material. J Occup Environ Hyg 9(5):308–318

Miller A, Frey G, King G, Sunderman C (2010) A handheld electrostatic precipitator for sampling airborne particles and nanoparticles. Aerosol Sci Technol 44(6):417–427

NIOSH (1994) Asbestos by TEM. Cincinnati, OH, Department of Health and Human Services, Centers for Disease Control and Prevention, National Institute for Occupational Safety and Health. NIOSH method 7402, issue 2

NIOSH (2008) Safe nanotechnology in the workplace. Cincinnati, Department of Health and Human Services, Centers for Disease Control and Prevention, National Institute for Occupational Safety and Health. NIOSH (DHHS) publication no, 2008-112

NIOSH (2009) Approaches to safe technology—managing the health and safety concerns associated with engineered nanomaterials. Cincinnati, OH, Department of Health and Human Services, Centers for Disease Control and Prevention, National Institute for Occupational Safety and Health. DHHS (NIOSH) publication no. 2009-125

NIOSH (2011) Occupational exposure to titanium dioxide. Cincinnati, Department of Health and Human Services, Centers for Disease Control and Prevention, National Institute for Occupational Safety and Health. DHHS (NIOSH) publication no. 2011-160

NIOSH (2013) Current intelligence bulletin 65—occupational exposure to carbon nanotubes and nanofibers. Cincinnati, Department of Health and Human Services, Centers for Disease Control and Prevention, National Institute for Occupational Safety and Health. DHHS (NIOSH) publication no. 2013-145

NSTC (2006) Environmental, health, and safety research needs for engineered nanoscale materials. Washington, D.C., National Science and technology council (NSTC), the National Nanotechnology Initiative, executive Office of the President of the United States

Oberdörster E (2004) Manufactured nanomaterials (fullerenes, C60) induce oxidative stress in the brain of juvenile largemouth bass. Environ Health Perspect 112(10):1058–1062

Park J, Kwak BK, Bae E, Lee J, Kim Y, Choi K, Yi J (2009) Characterization of exposure to silver nanoparticles in a manufacturing facility. J Nanopart Res 11(7):1705–1712

Roco MC (2003) Broader societal issues of nanotechnology. J Nanopart Res 5:181–189

Roco MC (2011) Erratum to: the long view of nanotechnology development: the National Nanotechnology Initiative at 10 years. J Nanopart Res 13:1335–1335

Schindelin J, Arganda-Carreras I, Frise E, Kaynig V, Longair M, Pietzsch T, Preibisch S, Rueden C, Saalfeld S, Schmid B (2012) Fiji: an open-source platform for biological-image analysis. Nat Methods 9(7):676–682

Schulte P, Geraci C, Zumwalde R, Hoover M, Castranova V, Kuempel E, Murashov V, Vainio H, Savolainen K (2008) Sharpening the focus on occupational safety and health in nanotechnology. Scand J Work Environ Health 34(6):407–409

Shvedova A, Castranova V, Kisin ER, Schwegler-Berry D, Murray AR, Gandelsman VZ, Maynard A, Baron P (2003) Exposure to carbon nanotube material: assessment of nanotube cytotoxicity using human keratinocyte cells. J Toxic Environ Health A 66:1909–1926

Sigma M (n.d.) GTTP02500 Isopore Membrane Filter. Jan. 2018

Simeonova PP, Opopol N, Luster MI (2007) Nanotechnology—toxicological issues and environmental safety. Springer, Dordrecht

Singh S, Nalwa HS (2007) Nanotechnology and health safety—toxicity and risk assessments of nanostructured materials on human health. J Nanosci Nanotechnol 7(9):3048–3070

Spurny K, Lodge J, Frank E, Sheesley D (1969) Aerosol filtration by means of Nuclepore filters structural and filtration properties. ES&T 3(5)

Su W-C, Vincent JH (2004) Experimental measurements and numerical calculations of aspiration efficiency for cylindrical thin-walled aerosol samplers in perfectly calm air. Aerosol Sci Technol 38(8)

Systems D (2017) ProX SLS 500. Retrieved from: https://www.3dsystems.com/3d-printers/prox-sls-500

Takagi A, Hirose A, Nishimura T, Fukumori N, Ogata A, Ohashi N, Kitajima S, Kanno J (2008) Induction of mesothelioma in p53+/− mouse by intraperitoneal application of multi-wall carbon nanotube. J Toxicol Sci 33(1):105–116

Takagi A, Hirose A, Futakuchi M, Tsuda H, Kanno J (2012) Dose-dependent mesothelioma induction by intraperitoneal administration of multi-wall carbon nanotubes in p53 heterozygous mice. Cancer Sci 103(8):1440–1444

Tsai SJ, Ada E, Isaacs J, Ellenbecker MJ (2009a) Airborne nanoparticle exposures associated with the manual handling of nanoalumina and nanosilver in fume hoods. J Nanopart Res 11(1):147–161

Tsai SJ, Hofmann M, Hallock M, Ada E, Kong J, Ellenbecker MJ (2009b) Characterization and evaluation of nanoparticle release during the synthesis of single-walled and multi-walled carbon nanotubes by chemical vapor deposition. Environ Sci Technol 43(15):6017–6023

Tsai CJ, Liu CN, Hung SM, Chen SC, Uang SN, Cheng YS, Zhou Y (2012) Novel active personal nanoparticle sampler for the exposure assessment of nanoparticles in workplaces. Environ Sci Technol 46(8):4546–4552

Twomey S (1962) Equations for the decay of diffusion of particles in an aerosol flowing through circular and rectangular channels. Bull Obs Puy de Dome 10

Warheit DB, Sayes CM, Reed KL, Swain KA (2008) Health effects related to nanoparticle exposures: environmental, health and safety considerations for assessing hazards and risks. Pharmacol Ther 120(1):35–42

Zarringhalam H, Hopkinson N, Kamperman NF, De Vlieger JJ (2006) Effects of processing on microstructure and properties of SLS nylon 12. Mater Sci Eng A (435)